BIOCHEMISTRY
including biophysical chemistry & molecular biology

Article

pubs.acs.org/biochemistry

The Qdot-Labeled Actin Super-Resolution Motility Assay Measures Low-Duty Cycle Muscle Myosin Step Size

Yihua Wang,[†] Katalin Ajtai,[†] and Thomas P. Burghardt*[,†,‡]

[†]Department of Biochemistry and Molecular Biology and [‡]Department of Physiology and Biomedical Engineering, Mayo Clinic Rochester, Rochester, Minnesota 55905, United States

Supporting Information

ABSTRACT: Myosin powers contraction in heart and skeletal muscle and is a leading target for mutations implicated in inheritable muscle diseases. During contraction, myosin transduces ATP free energy into the work of muscle shortening against resisting force. Muscle shortening involves relative sliding of myosin and actin filaments. Skeletal actin filaments were fluorescently labeled with a streptavidin conjugate quantum dot (Qdot) binding biotin-phalloidin on actin. Single Qdots were imaged in time with total internal reflection fluorescence microscopy and then spatially localized to 1−3 nm using a super-resolution algorithm as they translated with actin over a surface coated with skeletal heavy meromyosin (sHMM) or full-length β-cardiac myosin (MYH7). The average Qdot-actin velocity matches measurements with rhodamine-phalloidin-labeled actin. The sHMM Qdot-actin velocity histogram contains low-velocity events corresponding to actin translation in quantized steps of ∼5 nm. The MYH7 velocity histogram has quantized steps at 3 and 8 nm in addition to 5 nm and larger compliance compared to that of sHMM depending on the MYH7 surface concentration. Low-duty cycle skeletal and cardiac myosin present challenges for a single-molecule assay because actomyosin dissociates quickly and the freely moving element diffuses away. The in vitro motility assay has modestly more actomyosin interactions, and methylcellulose inhibited diffusion to sustain the complex while preserving a subset of encounters that do not overlap in time on a single actin filament. A single myosin step is isolated in time and space and then characterized using super-resolution. The approach provides a quick, quantitative, and inexpensive step size measurement for low-duty cycle muscle myosin.

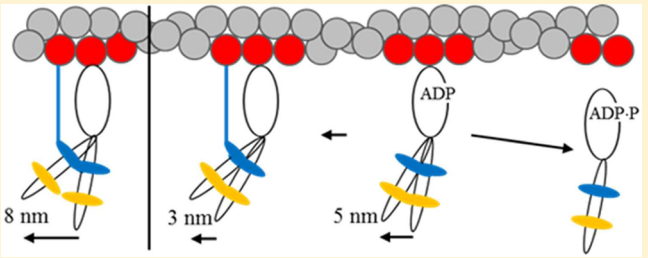

Myosin is a molecular motor powering the contraction of heart and skeletal muscle. It is frequently implicated in inheritable muscle diseases, including hypertrophic and dilated cardiomyopathy (HCM and DCM, respectively)[1] and skeletal muscle myopathies.[2] Characterizing myosin functionality and its alteration by disease-implicated mutation is a high priority because it elucidates the molecular basis for disease to identify the targets for smarter therapy. During contraction, myosin transduces chemical free energy in the form of ATP in the cell into the work of translating its force-producing partner actin against the force-resisting muscle shortening. Transduction and actin translation are principal myosin functionalities affected by disease. We are concerned here with actin translation quantitation.

Muscle myosin is a linear molecule with a globular head domain at the N-terminus containing the ATP and actin binding sites and a long tail that spontaneously associates into a two-headed dimer (both heads at one end). Head domain folding is assisted by two light chains, essential and regulatory, that bind to a long single α-helix in the head called the lever arm. Dimers form the rodlike myosin thick filament with excluded head domains that project outward toward adjacent actin thin filaments in a muscle fiber. Actin and myosin filaments slide relatively during contraction because of impulsive force by myosin that occurs while they are tightly bound to each other. Within the myosin head or subfragment 1 (S1), ATP hydrolysis drives rotary movement of the lever arm, converting rotation into the linear translation of actin.[3,4] The lever arm is stabilized by the two bound light chains, and they affect lever arm stiffness.[5] The single-ATPase cycle linear translation distance or step size, h, derives from the lever arm length and its shear stiffness. It is a crucial single-molecule parameter characterizing myosin functionality. The skeletal myosin crystal structure[3] and its homology-modeled analogue for cardiac myosin[6] indicate identical lever arm lengths for these isoforms, implying their identical step sizes.

The in vitro motility assay measures the velocity of actin gliding over a planar array of myosin immobilized on a surface. In its basic implementation, fluorescently labeled actin filaments glide over myosin to model unloaded contraction, producing maximal velocity actin movement. Myosin translates actin only while the two molecules are tightly bound. The myosin duty cycle is the ratio of the time spent with actin strongly bound, t_{on}, divided by the time to complete the ATPase cycle, τ. Muscle myosin has a low duty cycle, given by t_{on}/τ, to allow

Received: October 11, 2012
Revised: January 31, 2013
Published: February 5, 2013

   dx.doi.org/10.1021/bi301702p | *Biochemistry* 2013, 52, 1611−1621

rapid actin translation in a muscle fiber containing densely packed arrays of myosin motors interacting with translating actin filaments.[7,8] For low-duty cycle myosin, the actin sliding velocity in the motility assay depends on the myosin surface density because myosin is usually not actin-bound, so that many actomyosin interactions produce a longer actin translation between images of the fluorescent actin. A conventional microscope spatial resolution of ∼520 nm suggests >100 actomyosin interactions must occur between collected images for detection if h = 5.2 nm. The large number of actomyosin interactions required normally prohibits direct detection of h in the motility assay.

Sparse fluorescent probes individually imaged are localized to higher precision than diffraction-limited resolution by fitting the point spread function (PSF) to the measured photon distribution.[9,10] The analysis substitutes the distribution center for the point object position with precision determined by the signal-to-noise ratio (SNR) rather than the diffraction-limited PSF width.[11,12] This super-resolution imaging has localized point objects with <1 nm accuracy.[13] Low-duty cycle skeletal and cardiac myosins present challenges for a sparse single-molecule assay because actomyosin dissociates quickly and the freely moving element diffuses away. We introduce here super-resolution particle tracking of quantum dot (Qdot)-labeled actin in the standard in vitro motility assay. The in vitro motility assay has modestly more actomyosin interactions than a single-molecule encounter, while actin diffusion is inhibited by addition of methylcellulose to the motility buffer. The net effect sustains the actomyosin complex while preserving a subset of encounters that do not overlap in time on a single actin filament. A single myosin step is isolated in time and space and then characterized using super-resolution.

We immobilized rabbit skeletal heavy meromyosin (sHMM) on the planar substrate in the in vitro motility assay. Rapid sHMM motility limited camera exposure time to 10 ms to ensure actin is rarely actively translated by myosin during an exposure. This also determines practical limits for photon counts per pixel providing a spatial resolution of ∼3 nm for the actin-attached Qdot under the most favorable conditions. At a modest myosin surface density and actin filament length, quantized particle velocities corresponded to a unitary myosin step size of ∼5 nm for the low-duty cycle motor. We also immobilized full-length porcine β-cardiac myosin (MYH7) on the planar substrate in the in vitro motility assay. Its slower ATPase kinetics permitted a 30 ms exposure time, providing a spatial resolution minimum of ∼1 nm for the actin-attached Qdot under the most favorable conditions. For MYH7, we observed several unitary steps, one as expected at ∼5 nm and two less probable steps of 3 and 8 nm. The relative frequencies of the 3 and 5 nm steps are very different, making it unlikely that they are simply substeps of the longer 8 nm unitary step. Step sizes in MYH7 were shortened measurably at higher myosin surface concentrations, suggesting myosin compliance changes as myosin crowds the surface.

Quantitating in vitro motility velocity with super-resolution microscopy opens the way for rapid, quantitative, and inexpensive step size measurement in low-duty cycle muscle myosins implicated in inheritable muscle diseases.

MATERIALS AND METHODS

Chemicals. Quantum dot 585 streptavidin conjugate (Qdot), rhodamine-phalloidin, biotin-XX-phalloidin, and phalloidin were obtained from Life Technologies (Grand Island, NY). Glucose oxidase was purchased from MP Biomedicals (Santa Ana, CA). Biotin free bovine serum albumin (BSA, catalog no. A3059), catalase, and methylcellulose (m0262, molecular mass of 41 kDa) were from Sigma-Aldrich (St. Louis, MO). The Bradford assay was purchased from Bio-Rad (Hercules, CA). Other chemicals were purchased from Sigma-Aldrich or Affymetrix (Cleveland, OH).

sHMM Preparation. Rabbit skeletal myosin was prepared from the leg and back muscles by the method of Tonomura et al.[14] HMM was obtained by chymotryptic digestion of myosin.[15]

MYH7 Preparation. Porcine β-cardiac myosin (MYH7) was prepared from heart ventriculum as previously described for bovine cardiac myosin with some modifications.[16] MYH7 was extracted from minced, washed ventriculum for 10 min at 4 °C with a "Guba-Straub" solution [0.3 M KCl, 5 mM ATP, 1 mM DTT, 5 mM $MgCl_2$, and 1 mM EGTA in 50 mM potassium phosphate buffer (pH 6.5)]. After the solubilized myosin was separated from the tissue by centrifugation, three cycles of precipitation were performed to eliminate contaminating soluble proteins. Then the pellet was dissolved in a high-salt wash [0.6 M KCl, 5 mM ATP, 1 mM DTT, 5 mM $MgCl_2$, 1 mM EGTA, and 0.001 mg/mL leupeptin in 50 mM Tris-HCl (pH 8.0)] followed by ultracentrifugation (250000g for 2 h). The upper two-thirds of the supernatant was collected and dialyzed overnight in storage buffer [0.6 M KCl, 2 mM DTT, and 0.001 mg/mL leupeptin in 50 mM Tris-HCl (pH 7.4)] followed by ultracentrifugation (250000g for 3 h) to remove remaining actin or actomyosin impurities. MYH7 was stored in sealed tubes at −20 °C in 50% (v/v) glycerol.

Urea gel electrophoresis and mass spectrometry analysis of our porcine cardiac myosin did not detect any phosphorylated regulatory light chain (RLC) in the myosin.[17] The myosin has <5% actin impurity judged by analysis of the SYPRO Ruby-stained gel generated via sodium dodecyl sulfate−polyacrylamide gel electrophoresis.

Actin Preparation and Labeling. G-Actin was obtained from rabbit skeletal muscle acetone powder by using the method described by Pardee and Spudich[18] and then stored immediately under argon gas in liquid nitrogen. Before actin was used, the frozen G-actin was thawed and spun in an airfuge (Beckman Coulter, Indianapolis, IN) at 160000g for 90 min to remove denatured actin. We compared motilities of skeletal HMM using actin obtained with and without liquid nitrogen storage, and average velocities were the same within error. Rhodamine labeling of actin filaments was performed with rhodamine-phalloidin and actin in a 1.2:1 molar ratio as described previously.[19] Biotin-XX-phalloidin with rhodamine-phalloidin labeling of actin filaments was performed like rhodamine-phalloidin labeling but with a biotin-XX-phalloidin:rhodamine-phalloidin molar ratio of 1:9, while the total phalloidin derivative:actin molar ratio remained 1.2:1. We tested biotin-XX-phalloidin:rhodamine-phalloidin molar ratios of 1:1, 1:4, 1:9, 1:19, 1:49, 1:99, and 1:199 to optimize conditions favoring one Qdot per actin filament with most filaments labeled with Qdot and found 1:9 was optimal. Phalloidin derivatives were incubated with actin overnight on ice. Qdot streptavidin conjugation to the biotin-XX-phalloidin-labeled actin was conducted in the flow cell (see below).

sHMM in Vitro Motility. We removed sHMM dead-heads prior to use by mixing sHMM with phalloidin-labeled actin, adding 2 mM ATP, increasing the KCl concentration to 100 mM, and then spinning down the mixture at 160000g for 20

min.[20] Qdots (4 nM) were prepared in a Qdot solution (6% BSA in C buffer) just prior to the motility measurement using Qdot stock spun down at 5000*g*, and 1 μL of supernatant was added to 250 μL of a Qdot solution.

Motility assays using rhodamine-phalloidin-labeled actin filaments were performed as described by Kron et al.[19] We developed a protocol for the Qdot and rhodamine-phalloidin-labeled actin motility assay from Månsson et al.[21] with substantial changes. Each sHMM sample was diluted in C buffer [25 mM KCl, 25 mM imidazole (pH 7.4), 5 mM $MgCl_2$, 0.1 mM EGTA, 10 mM DTT, and 0.1 mM PMSF] to 0.057, 0.114, 0.171, or 0.285 μM (assuming a molecular mass for sHMM of 350 kDa), 15 μL of which was infused into a flow cell made from the nitrocellulose-coated glass coverslip and incubated for 2 min. After sHMM incubation, the flow cell was washed with 30 μL of a 1 mg/mL BSA solution (BSA in C buffer), incubated with 15 μL of a 25 mg/mL BSA solution for 2 min, and then washed again with 30 μL of a 1 mg/mL BSA solution. We conducted a second dead-head removal for sHMM immobilized in the flow cell by a 1 min incubation with 30 μL of C buffer, a 2 min incubation with 30 μL of 2 μM phalloidin-labeled actin in C buffer, a 1 min incubation with 30 μL of 1 mM ATP in C buffer, and a 1 min incubation with 30 μL of C buffer. After that, 30 μL of 4 nM biotin-XX-phalloidin with rhodamine-phalloidin-labeled actin in C buffer was infused for a 30 s incubation. Then, 30 μL of 4 nM Qdots in a Qdot solution was infused for a 60 s incubation. It was followed by a 30 μL volume of 1 μM biotin in C buffer to block free biotin binding sites on streptavidin. After a 1 min incubation, the flow cell was washed with 30 μL of C buffer and mounted on the microscope stage. Once the sample was in focus, the standard motility buffer [25 mM KCl, 25 mM imidazole (pH 7.4), 5 mM $MgCl_2$, 0.1 mM EGTA, 20 mM DTT, 0.1 mM PMSF, 0.7% methylcellulose with a viscosity of 12 cP at 20 °C, 2 mM ATP, 3 mg/mL glucose, 0.018 mg/mL catalase, and 0.1 mg/mL glucose oxidase] was infused to initiate motility. All the motility assays were performed at 21 °C.

MYH7 in Vitro Motility. In vitro motility assays for MYH7 using rhodamine-phalloidin-labeled actin were performed as previously described by Pant et al.[22] and Greenberg et al.[23] The assay using Qdot-labeled actin was similar to that for sHMM. MYH7 in 50% glycerol (200 μg of myosin) was suspended in 12 volumes of 10 mM DTT in ice-cold water, precipitated for 1 h on ice, and then centrifuged at 16000*g* for 30 min at 4 °C. The pellet was resuspended in 200 μL of M buffer [0.3 M KCl, 1 mM EGTA, 5 mM $MgCl_2$, and 10 mM DTT in 25 mM imidazole (pH 7.4)]. The myosin was mixed with 1 mM ATP and 1.1 μM actin in M buffer and centrifuged in an airfuge (100000*g* for 30 min) to remove dead-heads. The myosin concentration was determined using the Bradford assay, and then the sample was diluted to the desired concentration. Fifteen microliters of the myosin sample was infused into a flow cell made from the nitrocellulose-coated glass coverslip and incubated for 1 min. After incubation, the flow cell was washed with 30 μL of a 1 mg/mL BSA solution (BSA in M buffer), incubated with 15 μL of a 25 mg/mL BSA solution for 2 min, and then washed again with 30 μL of a 1 mg/mL BSA solution, followed by 90 μL of low-salt buffer [25 mM KCl, 1 mM EGTA, 5 mM $MgCl_2$, and 10 mM DTT in 25 mM imidazole (pH 7.4)]. After a 1 min incubation, we conducted a second dead-head removal by a 2 min incubation with 30 μL of 1 μM phalloidin-labeled actin in low-salt buffer, a 1 min incubation with 30 μL of 1 mM ATP in low-salt-buffer, and a 1 min incubation with 30 μL of low-salt buffer. After that, 30 μL of 8 nM biotin-XX-phalloidin and rhodamine-phalloidin-labeled actin in low-salt buffer was infused for a 30 s incubation. Then, 30 μL of 5 nM Qdots in a Qdot solution was infused for a 60 s incubation. It was followed by 30 μL of 1 μM biotin in low-salt buffer. After a 1 min incubation, the flow cell was washed with 30 μL of low-salt buffer and mounted on the microscope stage. Once the sample was in focus, the cardiac motility buffer [25 mM KCl, 25 mM imidazole (pH 7.4), 5 mM $MgCl_2$, 1 mM EGTA, 20 mM DTT, 0.7% methylcellulose, 2 mM ATP, 3 mg/mL glucose, 0.018 mg/mL catalase, and 0.1 mg/mL glucose oxidase] was infused to initiate motility.

Microscopy. Quantitative actin motility assays using Qdots always used the Qdot-labeled and rhodamine-phalloidin-labeled actin to allow evaluation of actin filament length and integrity. The in vitro motility of rhodamine-phalloidin or Qdot-labeled and rhodamine-phalloidin-labeled actin was observed with through-the-objective total internal reflection fluorescence (TIRF)[24] on an Olympus IX71 inverted microscope using a 150×, 1.45 NA objective. TIRF illumination is evanescent and confined to the flow cell surface containing sHMM or MYH7 with an ∼100 nm depth of penetration into the bulk phase. Images were acquired with an Andor EMCCD camera ($iXon_3$ 897 with 16 μm × 16 μm pixels and 16 bit dynamic range) at 20 frames per second and 10 ms exposures (sHMM) or 5 frames per second and 30 ms exposures (MYH7) using the software supplied by the manufacturer (SOLIS). Intensity values were converted to photons using the conversion formula in SOLIS as appropriate for our camera and the images output in TIFF format for reading into ImageJ. The argon ion laser (Coherent Innova 90C) intensity was ∼30 mW at 488 nm.

The total number of Qdot-labeled actin filaments observed decreased after infusion of motility buffer to ∼40% of its initial value in ∼5 min probably because of detachment from the surface and movement out of the evanescent illumination. This occurs sooner than the rhodamine-labeled actin filaments but long enough for completion of motility measurements.

Standard in vitro motility data were acquired from rhodamine-phalloidin-labeled actin or Qdot-labeled and rhodamine-phalloidin-labeled actin moving over sHMM or MYH7 using manual filament tracking with the ImageJ plugin MTrackJ.[25]

Super-Resolution Measurements. We processed photon-converted images for super-resolution using the QuickPALM ImageJ plugin super-resolution fitting algorithm in two dimensions.[26] The software identified and localized point objects that qualified for super-resolution fitting according to user specifications, including minimal SNR (>25 isolating Qdots) and maximal full width at half-maximum (fwhm) of 5 pixels (107 nm/pixel in object space for the 150× objective). QuickPALM analysis produced a table (SRTable) listing each qualifying particle, particle position in pixels, position standard deviation, and frame identifier. Using the SRTable, QuickPALM rendered the super-resolved particle data as single pixels per particle in the frame sequence of the original data. Two rendering types were used where each subsequential frame contained (i) no previously observed particle positions and (ii) all previously observed particle positions. The latter shows Qdot pathways that are useful during the manual particle tracking described below.

Type 2-rendered frames were read into ImageJ and analyzed with MTrackJ.[25] The single-pixel resolution (107 nm) of the rendered images is much lower than super-resolution (<10

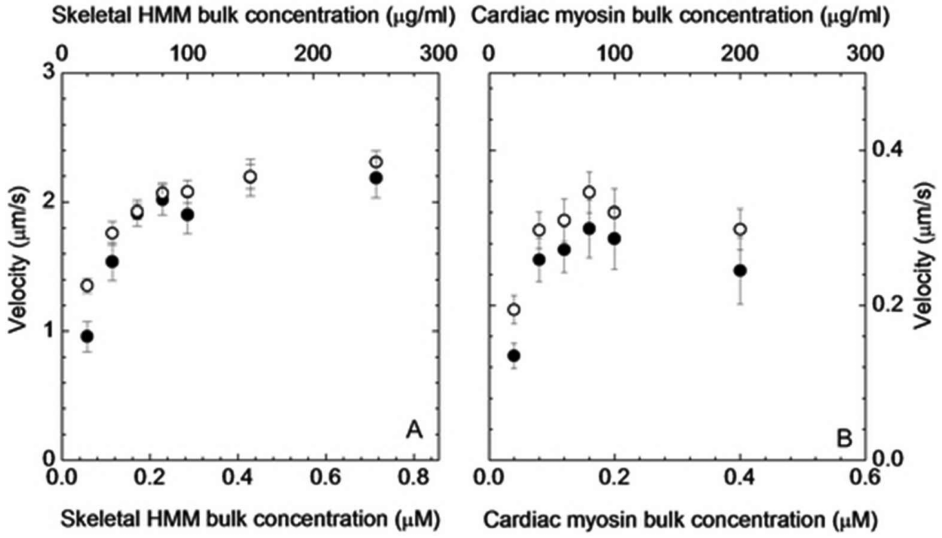

Figure 1. Ensemble average in vitro motility velocity vs bulk concentration of myosin for the rhodamine-phalloidin-labeled actin (○) and the Qdot-labeled and rhodamine-phalloidin-labeled actin (●). Error bars show the standard deviation: (A) sHMM and (B) MYH7.

nm). Manual tracking was needed only to link the super-resolved particle positions into a track connecting time-ordered frames. Manual tracking with MTrackJ provided a file identifying the approximate position (within a 3 pixel radius) of the super-resolved particle. A separate Mathematica program, SRTrack, linked the actual super-resolved particle coordinate to the track and then updated the SRTable with the frame-to-frame tracking-linked list. SRTrack eliminated any incorrectly identified MTrackJ particles that did not have a super-resolved equivalent. The latter removed the effect of Qdot blinking.

In any motility assay, a few Qdots did not visibly move because of apparent immobilization on the glass surface. These particles were tracked at super-resolution using the type 1-rendered images. Type 1-rendered images were treated like type 2-rendered images but used to analyze and quantitate thermal and mechanical fluctuations. These fluctuations were smaller than one pixel but were quantifiable at super-resolution. Stage drift was not detected in the velocity histograms used for data analysis probably because velocity data corresponded to the difference in Qdot positions between sequential frames.

Data Fitting. Measured Qdot velocities were plotted in histograms with velocity in units of $h/\Delta t = 1$, for h, the apparent step size parameter, and Δt, the frame capture time interval. Histogram intervals were 0.167−0.2 over the 0−4 velocity domain (20−25 intervals). The sHMM data separated into peaks by inspection corresponding approximately to 5 nm steps. Step size parameter h was then scanned over a 4 nm interval in small uniform steps (0.01 nm) with a median of 5 nm. The best step size was selected by minimizing the difference between peaks in the histogram and integer multiples of the initial peak near unit velocity. The MYH7 data separated into peaks by inspection, although the pattern was more complex than that for sHMM. The lowest-velocity peak was bimodal, corresponding to two steps, the longer and prevalent step near 5 nm and the shorter minor step near 3 nm. Step size was then scanned over a 4 nm interval in small uniform steps (0.01 nm) with a median of 4 nm. The best median step size was selected by minimizing the difference between peaks in the histogram and integer multiples of the prevalent step alone and in combination with the minor steps. We interpreted the prevalent step near 5 nm as unitary because of its anticipated correspondence with the unitary skeletal step. The sHMM did not indicate the minor step; hence, we attributed it to an unexpected difference between skeletal and cardiac isoforms, a consequence of full-length myosin in MYH7, or both possibilities. Our interpretation of the origin of the short step implies a third unitary step occurs at 8 nm as discussed in Results.

System Optimization. The machine setting for measuring step size with super-resolution in vitro motility optimizes the contrary requirements for point resolution and separating unitary actomyosin interactions in time. One method to do this is outlined here.

(1) Measure the ensemble average velocity using the super-resolution microscope and Qdot-labeled actin. The frame rate shows visible translation of actin between frames. Estimate motility velocity with standard resolution spot tracking. Optimize fluorescence collection efficiency to obtain the maximal number of photons for the lowest level of excitation light. Increase the excitation level to the maximum consistent with the probe photobleaching rate and the duration of the experiment. Qdots do not apparently photobleach; however, we needed to visualize both the Qdot and rhodamine label on the actin. This limits the excitation level.

(2) Analyze the standard motility data with QuickPALM. The program estimates and removes background light and computes the standard deviation for two spatial dimensions, (s_x, s_y), and signal intensity in photons ($N = \gamma t_e$), for t_e, the camera exposure time, and γ, the proportionality factor depending on excitation and detection characteristics. Assuming the x and y dimensions are equivalent, compute point resolution Δx (in pixels) using the relationship $\Delta x = [(s_x^2 + 1/12)/(\gamma t_e)]^{1/2}$.[11]

(3) Step size (h) measurement requires $\Delta x \sim h/2$, implying $t_e \gtrsim [4(s_x^2 + 1/12)]/(\gamma h^2)$. The time between successive frames $\Delta t > t_e$ for every camera. The cross-bridge produces actin translation during the actin attachment time, t_{on}, that is 2−20 ms for the skeletal and cardiac isoforms. The cross-bridge should not attach to actin during t_e to avoid a movement artifact. The probability that t_e and t_{on} overlap is $t_e \times t_{on}/(\Delta t)^2$ for the lowest-velocity events where the resolution is the most demanding. Overlap happens in this context ≤2% of the time under our conditions.

dx.doi.org/10.1021/bi301702p | *Biochemistry* 2013, 52, 1611−1621

(4) Isolating single cross-bridge interactions with actin during motility is most likely when Δt is small because it reduces the probability that two or more interactions will occur between successive frames. System optimization finds the smallest Δt consistent with what is described above.

(5) If the $\Delta x \sim h/2$ relationship cannot be satisfied, then increase the excitation level. Visualizing both the Qdot and rhodamine label on the actin is not an absolute requirement and does not need to be done continuously throughout the assay. For instance, check the actin filament length with rhodamine emission before the motility assay at a lowered exciting light level.

RESULTS

In Vitro Motility. Figure 1A shows the ensemble average sHMM motility velocity versus sHMM bulk concentration for the rhodamine-phalloidin-labeled actin (○) and Qdot-labeled and rhodamine-phalloidin-labeled actin (●). We used MTrackJ to do the manual tracking and average velocity calculation. Each filament was tracked for >20 μm. The sliding velocity of actin filaments at each sHMM concentration was measured by averaging the speeds of 25−40 filaments from two or three slides. Error bars show the standard deviation. The difference between the velocities of rhodamine-phalloidin-labeled actin and Qdot-labeled and rhodamine-phalloidin-labeled actin filaments was less than one standard deviation for sHMM bulk concentrations of ≥0.114 μM. The average motility velocity increases with increasing bulk sHMM concentration (and presumably with increasing sHMM surface density) as expected for a low-duty cycle motor. The divergence of velocities for rhodamine-phalloidin-labeled actin and Qdot-labeled and rhodamine-phalloidin-labeled actin at the lowest surface density suggests the Qdot imposes a force resisting movement for the static filament that is dispelled when the filament begins to move. Figure 1B shows the data equivalent to that in panel A for MYH7. MYH7 has maximal velocity that is approximately one-seventh of that of sHMM. The difference between the velocities of rhodamine-phalloidin-labeled actin and Qdot-labeled and rhodamine-phalloidin-labeled actin filaments was less than one standard deviation for MYH7 bulk concentrations of ≥0.08 μM, again implying the Qdot imposes a force resisting movement for the static filament that is dispelled when the filament begins to move. There is a small systematic reduction in velocity of ∼0.04 μm/s at all MYH7 bulk concentrations measured apparently imposed by the Qdot, suggesting a residual resisting force for the dynamic filament.

Figure 2 shows a single frame of Qdot-labeled and rhodamine-phalloidin-labeled actin filaments moving over surface-bound sHMM in a motility assay with a biotin-XX-phalloidin:rhodamine-phalloidin molar ratio of 1:9. Qdot intensity dominates the intensity scale in the figure, but the 16 bit dynamic range of the camera also captures a substantial intensity range for the rhodamine emission. The inset shows rhodamine-labeled actin filaments moving over surface-bound sHMM in a motility assay with a rhodamine-phalloidin:phalloidin molar ratio of 1:9. Rhodamine labeling is heterogeneous along the filament at this labeling density. Movies of Qdot-labeled and rhodamine-phalloidin-labeled actin moving over sHMM and MYH7 are available as Supporting Information.

Effect of Methylcellulose. Addition of 0.7% methylcellulose to the motility buffer was required to prevent actin filaments from diffusing from the myosin-coated surface while myosin density is low. It was shown previously that 0.5−1.0% methylcellulose in motility buffer increases the solution viscosity and retards the actin filament's lateral Brownian motion without significantly affecting the velocity of sliding over sHMM.[19,27] We found no difference in rhodamine-phalloidin-labeled actin velocity over MYH7 for 0.5 and 0.7% methylcellulose (data not shown, bulk MYH7 concentration of 0.1−0.2 μM).

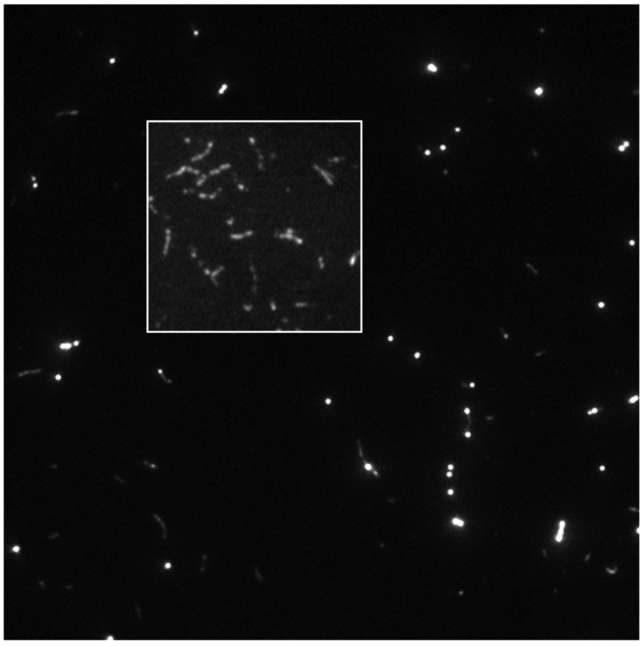

Figure 2. Qdot-labeled and rhodamine-phalloidin-labeled actin filaments bound to sHMM in the motility assay. The inset shows rhodamine-labeled actin filaments in the motility assay with a rhodamine-phalloidin:phalloidin molar ratio of 1:9. Rhodamine labeling is heterogeneous along the filament at this labeling density.

Super-Resolution Particle Tracking of sHMM. Figure 3 shows the type 2 rendering of an inverted-intensity super-resolved Qdot track in an in vitro motility assay. sHMM surface density, σ, derives from a bulk concentration of 0.114 μM. Each black square represents a 107 nm × 107 nm pixel containing the Qdot. Circles connected by a line mark the track manually created with MTrackJ. Super-resolved Qdot displacement among sequential frames is frequently within one rendered pixel, implying the rendered image will appear unchanged for two or more sequential frames. In this case, the MTrackJ user clicks on the same pixel over the frames with the unchanged image. This circumstance is indicated in Figure 3 with nearly concentric circles falling onto one pixel. MTrackJ writes the file identifying frame and circle position that is then linked to the actual super-resolved particle using these identifiers as described in Materials and Methods.

Figure 4 shows actin sliding velocity event distributions for sHMM in the low-velocity domain from 0 to 4.1 for h = 5.2 nm and frame capture interval Δt = 0.05 s (0−0.40 μm/s). Figure 4A shows the event distribution for σ derived from a 0.114 μM sHMM bulk solution (■) and baseline (●) from thermal and mechanical fluctuation events. Velocity probability data indicate discrete integer velocities corresponding to a myosin step size of 5.2 nm (Table 1). The area under the peaks at velocities 1−4 and after baseline subtraction corresponds to 8, 38, 40, and 66 events, respectively, for a total of 152 events. This sHMM bulk concentration was most efficient for producing the low-velocity

dx.doi.org/10.1021/bi301702p | Biochemistry 2013, 52, 1611−1621

Figure 3. High-contrast, intensity-inverted, Qdot track in an in vitro motility assay of sHMM. The QuickPALM super-resolved single particles are rendered at one pixel resolution, and all previously recorded frames are plotted in the image (type 2 rendering). Circles connected by a line mark the track manually created by MTrackJ. The circle is placed manually within a few pixels of the super-resolved particle position. The track is then associated with the correct super-resolved particle using another computer program, SRTrack, described in the text.

events providing the optimized sHMM surface density to favor nonoverlapping cross-bridge−actin interactions under our conditions. For this sample, the root-mean-square standard deviation (rmsd) in one dimension was as low as 3 nm, with an average value of 7 nm, for the point intensities recorded.[12]

Other bulk sHMM concentrations investigated produce similar velocity event recordings after baseline subtraction. Figure 4B combines events detected for σ derived from bulk concentrations of 0.057, 0.114, 0.171, and 0.285 μM for 497 total events. Event data at each bulk concentration had a fitted baseline from control immobilized Qdots subtracted to remove the thermal and mechanical fluctuation events as described below, and then velocity event distribution data were combined. Velocity histograms in Figure 4 were tabulated from two or three slides over 2−3 days with two data sets from each slide and for each bulk concentration. One data set contained 400−600 consecutive frames. Approximately 150 low-velocity events corresponding to 60−120 actin tracks were collected for each bulk concentration.

Simultaneously bound cross-bridges produce identical actin sliding velocities under unloaded conditions like those of the in vitro motility assay; hence, the net velocity is proportional to the time any cross-bridge is bound to actin between frames. Skeletal HMM has $1/\tau = V_{max} \sim 20$ s^{-1} [28] per cross-bridge and duty cycle $f \sim 0.05$,[7] implying the time spent with actin bound at the maximal sliding velocity is $t_{on} = f/V_{max} \sim 2.5$ ms. Two cross-bridges binding an actin filament at times offset by >3 ms

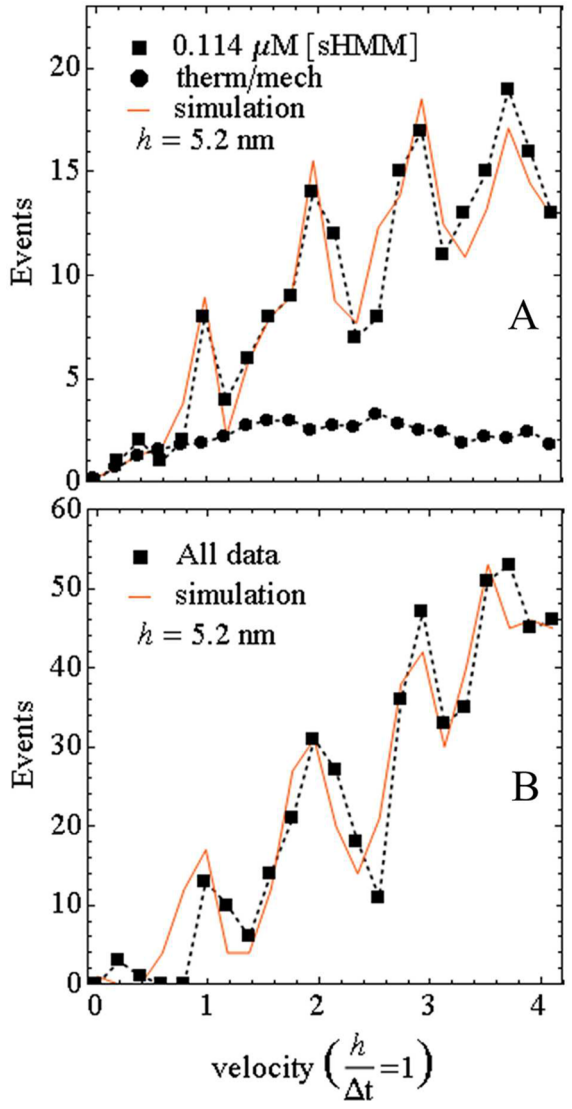

Figure 4. Actin sliding velocity event distribution for 50 ms frame capture intervals. (A) Event distribution for the 0.114 μM bulk sHMM solution (■ connected by a dashed line) and the simulation (solid line). The fitted baseline representing thermal and mechanical velocity fluctuation (● connected by a dashed line) is also shown. (B) Same as panel A except for the event distribution summed over all bulk concentrations. Simulated lines are generated as described in the text.

Table 1. Myosin in Vitro Step Sizes[a]

	unitary step size (nm)			step probability		
protein	1	2	3	1	2	3
sHMM	5.2	–	–	1	–	–
MYH7	5.1	8.2	3.2	1/2	3/8	1/8

[a]The error is ∼10% based on the goodness of fit for two-parameter (sHMM) or six-parameter (MYH7) fitting. Parameters are actin site occupation probability p, unitary step size, and (for MYH7) step probability.

but falling in the same frame capture interval will produce a sliding velocity of 2 (Figure 4). At a low actin sliding velocity, this is likely to occur. At higher velocities, where multiple cross-bridges are impelling actin, it is more likely that two or more cross-bridges will overlap some of their bound time, producing a net sliding velocity intermediate between the discrete

dx.doi.org/10.1021/bi301702p | Biochemistry 2013, 52, 1611−1621

velocities at or near 1−4. This effect is seen as the rising baseline in panels A and B of Figure 4 that is reproduced in the simulation.

We simulated motility assay velocity probability density using a time × space array representing an actin filament interacting with the surface-bound sHMM. Columns represent time evolution of myosin binding sites on actin. Rows are the spatial representation of myosin binding sites on actin located every 36 nm along the filament. They interact with surface-bound myosin. The binding site (or target zone) is three actin monomers long ($a \sim 16.5$ nm) and has a width w of ∼40 nm.[29] We simulated a 1.2 μm long actin filament having 33 total myosin binding sites (M). The time × space array was filled one row at a time by randomly generating binding site occupation from constant empty site occupation probability p that is the simulation parameter adjusted to match observation. We also tried an adapting algorithm where $p = p_0(M - g)/M$ for g, the number of occupied sites in the row, and p_0, the binding probability, when $g = 0$ under the assumption that tethering actin to the surface lowers the subsequent probability for binding due to steric constraints. For either algorithm, our expectation was that $p \propto \sigma a w$, implying p increases with an increasing sHMM bulk concentration, although this turned out to be incorrect as discussed below.

To evaluate time evolution, we partitioned t_{on} into n segments ($t_{seg} = t_{on}/n$); then using a $\langle t_{on} \rangle$ of 2.5 ms, we chose an actual on time for the bound cross-bridge randomly and normally distributed within a width that best reproduced the peak widths in panels A and B of Figure 4. For $n = 16$, a width of $2t_{seg}$ (∼0.3 ms) represented the observed dispersion in t_{on}. An occupied binding site remained occupied for several t_{seg}'s (one t_{seg} elapses between rows in the time × space array) and on average for $\langle t_{on} \rangle$. The total array column length is equal to $\Delta t/t_{seg}$, for Δt, the time interval between consecutive frames. The actin filament velocity is then the number of rows with at least one site occupied times the myosin step size divided by $n\Delta t$. The simulation for a single actin filament and for $\Delta t = 50$ ms is run repeatedly until the number of events falling in the 0−4 velocity range matches the number observed.

The baseline was fit to the velocity event distribution using the relationship $\mathbf{v}_{obs} = \mathbf{v}_{sim} + c\mathbf{v}_{t/m}$, where $\mathbf{v}_{obs}$ is the total observed column velocity event distribution vector, $\mathbf{v}_{sim}$ is the simulated equivalent to v_{obs} that does not include thermal and mechanical events, c is the unknown scalar, and $\mathbf{v}_{t/m}$ is the observed thermal and mechanical column velocity event distribution vector. Constant c is overdetermined and estimated by least-squares minimization with $c = \mathbf{v}_{t/m}{}^{T}(\mathbf{v}_{obs} - \mathbf{v}_{sim})/(\mathbf{v}_{t/m}{}^{T} \cdot \mathbf{v}_{t/m})$, where T means transpose.

Two scenarios creating low-velocity events have actin gliding over a homogeneous sHMM-coated surface whose coverage varies with the bulk sHMM concentration infused into the flow cell (implying p varies with the bulk sHMM concentration) but that occasionally produces a decrease in the amount of sHMM bound to the actin filament or a heterogeneous sHMM-coated surface whose average coverage varies with the bulk HMM concentration infused into the flow cell but where local low-density coverage areas are encountered (albeit less frequently with higher average sHMM coverage and implying a constant p). Simulation shows that a p of ∼0.0005 represented well the data for every surface concentration (Figure 4A,B), supporting the heterogeneous sHMM-coated surface scenario. Simulation shows that the homogeneous sHMM-coated surface scenario has discrete velocities heavily weighted toward the high-velocity end and contrasting with observation.

Simulated data are shown in panels A and B of Figure 4 as the solid line for 152 and 497 events (after baseline subtraction), respectively. The simulated areas under the peaks at 1−4 for a bulk concentration of 0.114 μM (Figure 4A) correspond to 9, 38, 46, and 58 events, respectively, that compare favorably to the 8-, 38-, 40-, and 66-event distributions observed. The total simulated and observed events are not identical because round-off from the baseline subtraction affects the two data sets differently. Peak areas for the combined data (Figure 4B) correspond to 29, 122, 116, and 230 and, 37, 125, 110, and 229 events, respectively, also demonstrating agreement between simulation and observation. At $p \sim 0.0005$, occupation probability was so low that a constant or adaptive p made no difference in the simulation.

Super-Resolution Particle Tracking of MYH7. Figure 5 shows actin sliding velocity event distributions for MYH7 in the low-velocity domain 0−4.1 in velocity units, where $h/\Delta t = 1$ for $h = 3.80$ (A), 3.3 (B), and 3.3 nm (C) and frame capture interval $\Delta t = 0.2$ s (0−0.08 or 0−0.07 μm/s). Figure 5A shows the event distribution for σ derived from an MYH7 bulk concentration of 0.08 μM (■) and baseline (●) from thermal and mechanical fluctuation events. Velocity probability data indicate discrete integer velocities corresponding to three myosin step sizes of ∼3.2, ∼5.1, and ∼8.2 nm (different sized single vertical arrows in Figure 5A). The total area under the curve in Figure 5A corresponds to 436 events. For this sample, the rmsd in one dimension was as low as 1 nm, with an average value of 2.4 nm, for the point intensities recorded.[12]

Other higher bulk MYH7 concentrations investigated produce velocity event recordings indicating diminishing unitary step sizes for increasing bulk concentrations. Panels B and C show the actin sliding velocity event distributions from 0.12 and 0.16 μM MYH7 (■) and the baseline (●) from thermal and mechanical fluctuations. The unitary step size decreases by ∼22% as the MYH7 concentration increases from 0.08 to 0.16 μM. It suggests myosin compliance changes with a diminished level of direct contact with the planar surface as myosin crowds the surface. More MYH7 compliance at a higher surface density also explains the slightly diminished ensemble average velocity at higher MYH7 concentrations seen in Figure 1.

Simulated velocity histograms are depicted with the solid lines in Figure 5. The 8 nm peak is similar in length to the short and medium steps in combination (indicated in the smaller font below the curve); hence, we used simulation to investigate the relative contributions of the combined steps and unitary 8 nm step to the 8 nm peak. Multiple step sizes were programmed into the time × space array by assigning each actin binding event with a unitary step size selected randomly from a weighted list. Step size list {3, 5, 8} nm or {3, 5} nm had weights and step sizes adjusted for best fitting. Simulations with the two- or three-step lists are otherwise identical. Step length/weight {3.2, 5.1, 8.2}/{1/8, 1/2, 3/8} or {3.2, 5.1}/{1/5, 4/5} coordinates provided best fits with the step list, including the preferred 8.2 nm unitary step (red line). Without the 8.2 nm unitary step, best fitting causes the simulation to substantially overshoot the 3.2 and 5.1 nm peaks in the event histogram (blue line), indicating the event deficit at 8.2 nm. The peak assigned to the combined 5.1 and 8.2 nm steps is substantially underoccupied in the blue line simulation, again demonstrating the need for the unitary 8.2 nm step. Step weighting {1/8, 1/2,

dx.doi.org/10.1021/bi301702p | Biochemistry 2013, 52, 1611−1621

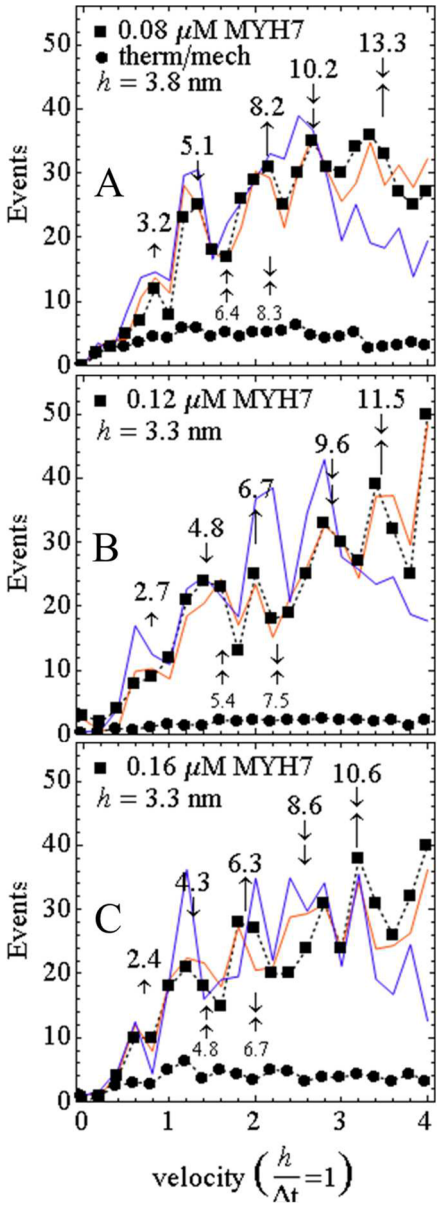

Figure 5. Actin sliding velocity event distribution for 200 ms frame capture intervals. Single vertical arrows identify unitary steps (short, medium, and long), and their correlation to peaks in the velocity histogram. The orientation of the arrow (up or down) is shown for the sake of clarity and has no significance. Combined vertical arrows indicate multiple unitary step combinations. Numbers above the vertical arrows indicate observed steps in nanometers computed by multiplying the ordinate position by the step parameter h. Smaller font step lengths below the curves are two short or one short−one medium combinations that are often not evidentially present in the experimental data. (A) Event distribution for the bulk MYH7 concentration of 0.08 μM (■ connected by a dashed line) and simulations (solid lines). Simulations include two (blue) or three (red) unitary steps. Fitting parameter h = 3.8. The fitted baseline (● connected by a dashed line) represents thermal and mechanical velocity fluctuation. (B and C) Same as in panel A except for bulk MYH7 concentrations of 0.12 and 0.16 μM and fitting parameter h = 3.3.

3/8} indicates 5.1 nm is the major step, 8.2 nm nearly as likely, and 3.2 nm least likely. Similar simulation results were obtained for the higher-MYH7 concentration curves with the shorter unitary steps sizes indicated. An occupation probability p of ∼0.00065 for all MYH7 concentrations indicates the heterogeneous MYH7-coated surface scenario like that suggested for sHMM. Occupation probability is somewhat higher than the sHMM concentration, consistent with a higher duty cycle.

Velocity event distributions in Figure 5 were tabulated from two or three slides over 2−3 days with two data sets from each slide and for each bulk concentration. One data set contained 200−400 consecutive frames. Approximately 400 low-velocity events corresponding to 60−120 actin tracks were collected for each bulk concentration.

DISCUSSION

The in vitro motility assay is a versatile and ubiquitous protein assay that, at the time of its introduction, distinctively altered how we characterized motor protein functionality.[30] The assay has changed format and complexity over the years and continues to play an important role in motor protein characterization for classification and elucidation of structure and function. The various myosin ATPases and in vitro motility draw a broadly based picture of motor protein behavior, marking the beginning and ending of energy transduction. Our objective here was to introduce super-resolution particle tracking to the assay and develop a quick, quantitative, and cheap method for detecting a single myosin step size in a low-duty cycle motor. Measuring actin movement with a low-duty cycle motor in a single-molecule assay in which one motor protein binds actin presents challenges because actomyosin will quickly dissociate and the freely moving element (myosin or actin) will diffuse away. We show that the motility assay allows modestly more actomyosin interactions that, together with the methylcellulose-inhibited diffusion, keeps actin from diffusing away without causing overlapping interactions such that a single myosin step is isolated in time. Super-resolution microscopy permits quantitation of the below diffraction limit translation by a single step.

Quantized actin filament sliding velocity was detected in the in vitro motility assay years ago.[7] The slow quantized velocities, attributed to single myosin interactions with the actin filament, were detected with fluorescence using a spatial localization method conceptually identical to super-resolution. Results suggested the actin localization accuracy was ∼14 nm and that the rabbit skeletal myosin cross-bridge step size was 5−20 nm. Later, using a different microscope-based technology, mechanical measurements detected actin binding of S1 immobilized on a spherical bead. The S1 was constrained to interact repeatedly with a single actin filament stretched between dielectric spheres held in laser traps. This setup had nanometer spatial and piconewton force resolutions and a measured step size of ∼5.2 nm for rabbit skeletal S1.[29]

In this work, we returned to the standard motility assay while introducing two relatively recent technical innovations. Qdot labeling of actin via a biotin-streptavidin linker introduces a photostable and very bright point source probe.[31] Visualization of the actin filament labeled with the Qdot and rhodamine-phalloidin shows that the Qdot sparsely labels intact filaments that translate over surface-bound sHMM. A similar average in vitro actin motility velocity for pure rhodamine-phalloidin-labeled actin versus Qdot-labeled and rhodamine-phalloidin-labeled actin shows that the Qdot does not alter motility. Qdot labeling facilitates application of the super-resolution method to spatially localize the label to below the diffraction limit. For sHMM, an EMCCD camera capturing one frame per 50 ms

quantified Qdot-labeled actin motility. Images analyzed with QuickPALM[26] produced Qdot localization with a spatial resolution approaching 3 nm in the most favorable cases. Qdot localization data linked frame by frame to actin motility tracks were interpreted by velocity histograms depicting the low-velocity domain where one to four cross-bridges produce actin translation measured as velocity by dividing the distance traveled by the 50 ms frame rate. In this velocity domain, discrete peaks mark the expected velocity for a 5.2 nm step size actomyosin interaction. We also find that the peak amplitudes are independent of myosin surface density over the coverage range caused by bulk sHMM concentrations from 0.057 to 0.285 μM, implying that under these experimental conditions the actin filaments interact with a heterogeneous myosin-coated surface that is frequently locally sparse. Actin motility simulation indicates the shape of the velocity distribution curve is determined by step size and t_{on} as peaks are located in multiples of the step size divided by the frame rate and the rising baseline at higher velocity is due to cross-bridge binding events that overlap in time. We found no evidence of cooperation between sHMM heads but expected this to be manifest as anomalously high amplitude peaks at velocities 2, 3, and 4 because of accelerated binding of second heads.

We also investigated the in vitro motility of cardiac myosin MYH7. This motor also moves the Qdot- and rhodamine-labeled actin and rhodamine-labeled actin with equivalent efficiency. The ensemble average motility velocity slows by a factor of 7 compared to that of sHMM, allowing a slower frame capture rate to follow movement and longer exposure time light collection. QuickPALM produced Qdot localization with spatial resolution approaching 1 nm in the most favorable cases. The MYH7 low-velocity histogram indicates three unitary step sizes of 3.2, 5.1, and 8.2 nm at 0.08 μM MYH7 with weighting {1/8, 1/2, 3/8} (independent of MYH7 concentration). Inspection of Figure 5A indicates that the relative frequencies of the 3 and 5 nm steps are very different, making it unlikely that they are parts of the same longer unitary step of 8 nm. We propose that the major 5 nm step is the default step and identical to the unitary step in sHMM. The 8 nm step is somewhat less likely and possibly different from the 5 nm step because the former involves an extra interaction with actin via the essential light chain (ELC). The cardiac ELC is known to bind actin by a unique N-terminal extension.[32,33] Our data show the 5 and 8 nm steps make up seven of the eight steps in the MYH7 in vitro motility assay. The minor 3 nm step is the unlikely conversion of the 5 nm step to the full ELC-bound 8 nm step. It occurs in just one of eight cycles and is isolated in time from the 5 nm step by the ADP dissociation time; hence, we observe it as an independent step.

Figure 6 shows the proposed three-step mechanism for MYH7 and partial elements of the time × space array used for the simulation. Slow ADP release in the majority cross-bridge is indicated for the 5 nm step cycle shown. Columns of the time × space array are indicated for each actin binding target zone shown and for three Δt values. In an actual simulation, columns contain 200 elements for Δt = 200 ms and t_{seg} = 1 ms. For the indicated Δt intervals, we would record Qdot translations of 5, 8, and 8 nm with the first translation due to the unitary 5 nm step, the second translation the result of combined 3 and 5 nm displacements from two different cross-bridges, and the third the unitary 8 nm step of a single cross-bridge. The 3, 5, and 8 nm steps are independent in the simulation, although the 3 and

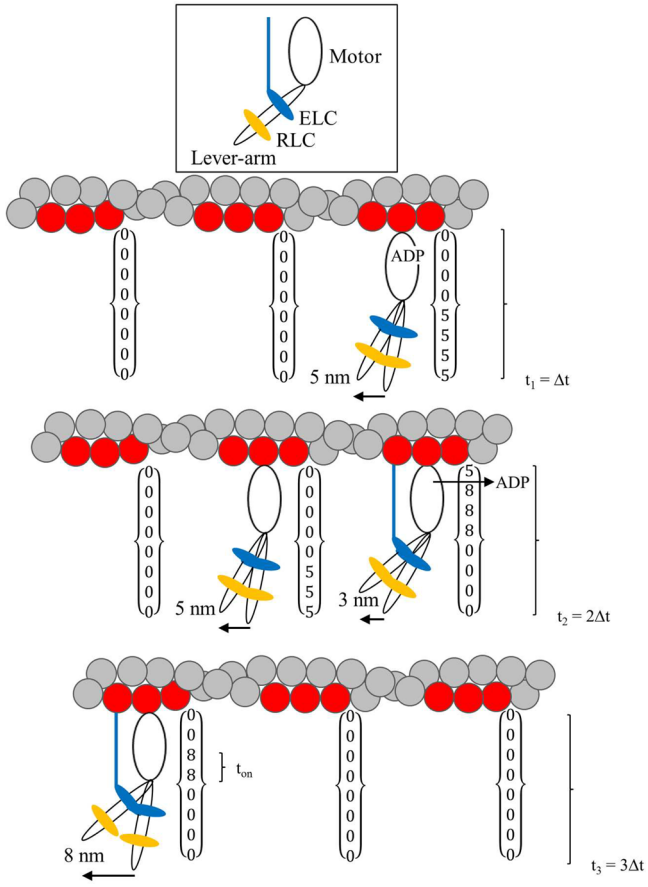

Figure 6. Three steps of MYH7 and their representation in the time × space array used in the simulation. The MYH7 cross-bridge has a motor domain, lever arm, and two light chains, ELC (blue) and RLC (orange), indicated at the top. The actin−ELC linkage, shown as a line connecting ELC with actin, modulates myosin step size. The three actin monomers in the target zone are colored red. Each target zone has a column in the time × space array. The figure shows three frame capture intervals, Δt, with frame capture happening at $t = t_1$, t_2, and t_3. The cross-bridge attached at the top right performs the major 5 nm step giving the 5 nm displacement recorded at t_1. Slow ADP release is indicated in the 5 nm step cycle shown. This cross-bridge remains attached into the second exposure interval when it releases ADP and then converts to the 8 nm step with the ELC linkage and produces the minor 3 nm displacement. Additional displacement of 5 nm by the middle cross-bridge releases ADP without the ELC linkage in the second exposure interval, giving 3 + 5 nm total displacement at t_2 due to two different unitary steps. The third exposure interval has a unitary 8 nm displacement caused by a minor step from a single cross-bridge.

5 nm steps are coupled in the mechanism proposed in Figure 6. Future work will investigate coupling between these events.

Modulating probability for short or long power strokes would affect sliding velocity and provide a mechanism for fine-tuning efficiency for a dynamic work load. For the mechanism in Figure 6, step length modulation is accomplished by guiding the ELC−actin linkage. This could involve either thick or thin filament regulation. On the thick filament, myosin RLC binds to the myosin lever arm and stiffens its resistance to deformation.[23,34] RLC phosphorylation is known to impact the resting head posture relative to the myosin filament backbone[35] and is implicated in cardiac contractility regulation.[36] RLC disease-implicated mutation was suggested to affect actin binding potentially via the ELC extension.[34] Cardiac

dx.doi.org/10.1021/bi301702p | *Biochemistry* 2013, 52, 1611−1621

myosin regulation by RLC could rest on the ability of RLC to modulate step size in an active muscle. In experiments reported here, MYH7 was not phosphorylated.[17]

Seiryo et al. compared step sizes for the rat α- and β-cardiac myosins and reported a single unitary step of 8−9 nm for both isoforms.[37] Palmiter et al. compared step sizes for the rabbit α- and β-cardiac myosins and reported a single unitary 7.2 ± 3.1 nm step for the β-isoform.[38] More recent work with rabbit cardiac myosin and regulated actin reported a 7 ± 3 nm unitary displacement.[39] The extent of myosin phosphorylation was not reported. These cardiac myosin unitary displacements are consistent with the 6.0 nm weighted average of our three steps. Whether our three-step scenario is consistent with this earlier work needs to be investigated further.

Application of super-resolution in vitro motility to disease-implicated mutations in the myosin heavy and light chains in low-duty cycle muscle myosin will uniquely elucidate the effect of mutation on step size. The skeletal and cardiac myosin applications described here dramatically demonstrate the power of the technique and its ability to distinguish and quantify subtle changes in the velocity due to step size alteration. We have demonstrated a rapid, practical, and sensitive assay for myosin step size that has already provided interesting new insights into contractility.

■ ASSOCIATED CONTENT

Supporting Information

The 20 s real time movie (17sHMM) shows Qdot- and rhodamine-labeled actin filaments moving over rabbit skeletal HMM immobilized on the nitrocellulose-coated glass surface. Surface-bound sHMM derives from a bulk sHMM concentration of 0.114 μM. The 80 s real time movie (419MYH7) shows Qdot- and rhodamine-labeled actin filaments moving over cardiac myosin immobilized on the nitrocellulose-coated glass surface. Surface-bound myosin derives from a bulk MYH7 concentration of 0.08 μM. Emission is dominated by the single Qdots, but the rhodamine label is also visible. Rhodamine labeling is sparse with single rhodamines on the actin sometimes recognizable. This material is available free of charge via the Internet at http://pubs.acs.org.

■ AUTHOR INFORMATION

Corresponding Author

*Department of Biochemistry and Molecular Biology and Department of Physiology and Biomedical Engineering, Mayo Clinic Rochester, Rochester, MN 55905. Telephone: (507) 284-8120. Fax: (507) 284-9349. E-mail: burghardt@mayo.edu.

Funding

This work was supported by National Institutes of Health Grants R01AR049277 and R01HL095572 and by the Mayo Foundation.

Notes

The authors declare no competing financial interest.

■ ACKNOWLEDGMENTS

Thanks to Brian Haldeman (University of Nevada, Reno, NV) for suggesting biotin-free BSA.

■ REFERENCES

(1) Moore, J. R., Leinwand, L., and Warshaw, D. M. (2012) Understanding Cardiomyopathy Phenotypes Based on the Functional Impact of Mutations in the Myosin Motor. *Circ. Res. 111*, 375−385.

(2) Tajsharghi, H., Kimber, E., Kroksmark, A. K., Jerre, R., Tulinius, M., and Oldfors, A. (2008) Embryonic Myosin Heavy-Chain Mutations Cause Distal Arthrogryposis and Developmental Myosin Myopathy That Persists Postnatally. *Arch. Neurol. 65*, 1083−1090.

(3) Rayment, I., Rypniewski, W. R., Schmidt-Base, K., Smith, R., Tomchick, D. R., Benning, M. M., Winkelmann, D. A., Wesenberg, G., and Holden, H. M. (1993) Three-dimensional structure of myosin subfragment-1: A molecular motor. *Science 261*, 50−58.

(4) Dominguez, R., Freyzon, Y., Trybus, K. M., and Cohen, C. (1998) Crystal structure of a vertebrate smooth muscle myosin motor domain and its complex with the essential light chain: Visualization of the pre-power stroke state. *Cell 94*, 559−571.

(5) Sherwood, J. J., Waller, G. S., Warshaw, D. M., and Lowey, S. (2004) A point mutation in the regulatory light chain reduces the step size of skeletal muscle myosin. *Proc. Natl. Acad. Sci. U.S.A. 101*, 10973−10978.

(6) Burghardt, T. P., Josephson, M. P., and Ajtai, K. (2011) Single myosin cross-bridge orientation in cardiac papillary muscle detects lever-arm shear strain in transduction. *Biochemistry 50*, 7809−7821.

(7) Uyeda, T. Q. P., Warrick, H. M., Kron, S. J., and Spudich, J. A. (1991) Quantized velocities at low myosin densities in an in vitro motility assay. *Nature 352*, 307−311.

(8) O'Connell, C. B., Tyska, M. J., and Mooseker, M. S. (2007) Myosin at work: Motor adaptations for a variety of cellular functions. *Biochim. Biophys. Acta 1773*, 615−630.

(9) Betzig, E., Patterson, G. H., Sougrat, R., Lindwasser, O. W., Olenych, S., Bonifacino, J. S., Davidson, M. W., Lippincott-Schwartz, J., and Hess, H. F. (2006) Imaging intracellular fluorescent proteins at nanometer resolution. *Science 313*, 1642−1645.

(10) Rust, M. J., Bates, M., and Zhuang, X. (2006) Sub-diffraction-limit imaging by stochastic optical reconstruction microscopy (STORM). *Nat. Methods 3*, 793−795.

(11) Bobroff, N. (1986) Position measurement with a resolution and noise-limited instrument. *Rev. Sci. Instrum. 57*, 1152−1157.

(12) Thompson, R. E., Larson, D. R., and Webb, W. W. (2002) Precise nanometer localization analysis for individual fluorescent probes. *Biophys. J. 82*, 2775−2783.

(13) Pertsinidis, A., Zhang, Y., and Chu, S. (2010) Subnanometre single-molecule localization, registration and distance measurements. *Nature 466*, 647−651.

(14) Tonomura, Y., Appel, P., and Morales, M. (1966) On the molecular weight of myosin II. *Biochemistry 5*, 515−521.

(15) Weeds, A. G., and Taylor, R. S. (1975) Separation of subfragment-1 isoenzymes from rabbit skeletal muscle myosin. *Nature 257*, 54−56.

(16) Ajtai, K., Garamszegi, S. P., Park, S., Velazquez Dones, A. L., and Burghardt, T. P. (2001) Structural characterization of β-cardiac myosin subfragment 1 in solution. *Biochemistry 40*, 12078−12093.

(17) Josephson, M. P., Sikkink, L. A., Penheiter, A. R., Burghardt, T. P., and Ajtai, K. (2011) Smooth muscle myosin light chain kinase efficiently phosphorylates serine 15 of cardiac myosin regulatory light chain. *Biochem. Biophys. Res. Commun. 416*, 367−371.

(18) Pardee, J. D., and Spudich, J. A. (1982) Purification of muscle actin. *Methods Enzymol. 85*, 164−179.

(19) Kron, S. J., Toyoshima, Y. Y., Uyeda, T. Q. P., and Spudich, J. A. (1991) Assays for actin sliding movement over myosin-coated surfaces. *Methods Enzymol. 196*, 399−416.

(20) Trybus, K. M. (2000) Biochemical studies of myosin. *Methods 22*, 327−335.

(21) Månsson, A., Sundberg, M., Balaz, M., Bunk, R., Nicholls, I. A., Omling, P., Tågerud, S., and Montelius, L. (2004) In vitro sliding of actin filaments labelled with single quantum dots. *Biochem. Biophys. Res. Commun. 314*, 529−534.

(22) Pant, K., Watt, J., Greenberg, M., Jones, M., Szczesna-Cordary, D., and Moore, J. R. (2009) Removal of the cardiac myosin regulatory light chain increases isometric force production. *FASEB J. 23*, 3571−3580.

(23) Greenberg, M. J., Watt, J. D., Jones, M., Kazmierczak, K., Szczesna-Cordary, D., and Moore, J. R. (2009) Regulatory light chain

mutations associated with cardiomyopathy affect myosin mechanics and kinetics. *J. Mol. Cell. Cardiol. 46*, 108−115.
(24) Stout, A. L., and Axelrod, D. (1989) Evanescent field excitation of fluorescence by epi-illumination microscopy. *Appl. Opt. 28*, 5237−5242.
(25) Meijering, E., Dzyubachyk, O., and Smal, I. (2012) Methods for Cell and Particle Tracking. In *Methods in Enzymology* (Conn, P. M., Ed.) Chapter 9, pp 183−200, Academic Press, New York.
(26) Henriques, R., Lelek, M., Fornasiero, E. F., Valtorta, F., Zimmer, C., and Mhlanga, M. M. (2010) QuickPALM: 3D real-time photoactivation nanoscopy image processing in ImageJ. *Nat. Methods 7*, 339−340.
(27) Uyeda, T. Q. P., Kron, S. J., and Spudich, J. A. (1990) Myosin step size: Estimation from slow sliding movement of actin over low densities of heavy meromyosin. *J. Mol. Biol. 214*, 699−710.
(28) Muhlrad, A., Peyser, Y. M., Nili, M., Ajtai, K., Reisler, E., and Burghardt, T. P. (2003) Chemical decoupling of ATPase activation and force production from the contractile cycle in myosin by steric hindrance of lever arm movement. *Biophys. J. 84*, 1047−1056.
(29) Steffen, W., Smith, D., Simmons, R., and Sleep, J. (2001) Mapping the actin filament with myosin. *Proc. Natl. Acad. Sci. U.S.A. 98*, 14949−14954.
(30) Sheetz, M. P., and Spudich, J. A. (1983) Movement of myosin-coated fluorescent beads on actin cables in vitro. *Nature 303*, 31−35.
(31) Medintz, I. L., Uyeda, H. T., Goldman, E. R., and Mattoussi, H. (2005) Quantum dot bioconjugates for imaging, labelling and sensing. *Nat. Mater. 4*, 435−446.
(32) Miyanishi, T., Ishikawa, T., Hayashibara, T., Maita, T., and Wakabayashi, T. (2002) The two actin-binding regions on the myosin heads of cardiac muscle. *Biochemistry 41*, 5429−5438.
(33) Schaub, M. C., Hefti, M. A., Zuellig, R. A., and Morano, I. (1998) Modulation of contractility in human cardiac hypertrophy by myosin essential light chain isoforms. *Cardiovasc. Res. 37*, 381−404.
(34) Burghardt, T. P., and Sikkink, L. A. (2013) Regulatory Light Chain Mutants Linked to Heart Disease Modify the Cardiac Myosin Lever-Arm. *Biochemistry 52*, 1249−1259.
(35) Sheikh, F., Ouyang, K., Campbell, S. G., Lyon, R. C., Chuang, J., Fitzsimons, D., Tangney, J., Hidalgo, C. G., Chung, C. S., Cheng, H., Dalton, N. D., Gu, Y., Kasahara, H., Ghassemian, M., Omens, J. H., Peterson, K. L., Granzier, H. L., Moss, R. L., McCulloch, A. D., and Chen, J. (2012) Mouse and computational models link Mlc2v dephosphorylation to altered myosin kinetics in early cardiac disease. *J. Clin. Invest. 122*, 1209−1221.
(36) Scruggs, S. B., and Solaro, R. J. (2011) The signficiance of regulatory light chain phosphorylation in cardiac physiology. *Arch. Biochem. Biophys. 510*, 129−134.
(37) Sugiura, S., Kobayakawa, N., Fujita, H., Yamashita, H., Momomura, S.-i., Chaen, S., Omata, M., and Sugi, H. (1998) Comparison of Unitary Displacements and Forces Between 2 Cardiac Myosin Isoforms by the Optical Trap Technique: Molecular Basis for Cardiac Adaptation. *Circ. Res. 82*, 1029−1034.
(38) Palmiter, K. A., Tyska, M. J., Dupuis, D. E., Alpert, N. R., and Warshaw, D. M. (1999) Kinetic differences at the single molecule level account for the functional diversity of rabbit cardiac myosin isoforms. *J. Physiol. 519*, 669−678.
(39) Debold, E. P., Saber, W., Cheema, Y., Bookwalter, C. S., Trybus, K. M., Warshaw, D. M., and VanBuren, P. (2010) Human actin mutations associated with hypertrophic and dilated cardiomyopathies demonstrate distinct thin filament regulatory properties in vitro. *J. Mol. Cell. Cardiol. 48*, 286−292.